Magnetic properties of bct Fe_xMn_{1-x} thin-film alloys investigated by linearly polarized soft-x-ray resonant magnetic reflectivity

A. Déchelette, J. M. Tonnerre, M. C. Saint Lager, F. Bartolomé, L. Sève, and D. Raoux
Laboratoire de Cristallographie, CNRS/Université J. Fourier, Boîte Postale 166, 38042 Grenoble Cedex 9, France

H. Fischer and M. Piecuch
Laboratoire de Métallurgie Physique et Sciences des Matériaux, CNRS/Université Henri Poincaré, Boîte Postale 239, 54506 Vandœuvre-lès-Nancy, France

V. Chakarian
Naval Research Laboratory, Washington, DC 20375

C. C. Kao
National Synchrotron Light Source, Brookhaven National Laboratory, Upton, New York 11973
(Received 12 March 1998; revised manuscript received 12 May 1999)

The magnetic properties of Fe_xMn_{1-x}/Ir(001) superlattices (SL's) have been studied using linearly polarized soft x-ray resonant magnetic reflectivity (XRMS) at the Fe $L_{2,3}$ absorption edges. Previous superconducting quantum interference device magnetometry measurements have shown that the SL's exhibit a ferromagnetic behavior for $x>0.75$ and a nonmagnetic or antiferromagnetic one for $x<0.75$. XRMS measurements were performed on two SL's with compositions on each side of $x=0.75$, as well as on a thin layer of Fe-rich alloy ($x=0.9$). The Fe magnetic moments in these alloys were determined by comparing experimental and calculated energy-dependent asymmetry ratios at different angles in the reflectivity curves. Fe atoms are found in a high-spin ferromagnetic state for $x=0.9$, while they are in a low-spin ferromagnetic state for $x=0.7$. Our results emphasize the role of the tetragonalization parameter c/a on the occurrence of the different magnetic states. Measurements, at the Mn $L_{2,3}$ edges in a bct $Fe_{0.9}Mn_{0.1}$ ultrathin layer reveal a net magnetic moment per Mn atom of about $1.7\mu_B$ coupled antiparallel to the Fe one. [S0163-1829(99)03933-8]

I. INTRODUCTION

The magnetic properties of thin films and artificial structures such as superlattices are nowadays widely investigated.[1,2] Among the different possibilities offered by these artificial systems, the stablilization of new phases induced by epitaxial strain is particularly interesting because they can exhibit physical properties different from those of bulk materials.

Elemental iron and manganese exist in various forms and their fcc phase has drawn much attention because magnetovolume effects have been predicted for both compounds.[3] However, Fe and Mn fcc phases have a limited stability range (1184–1665 K for fcc-Fe and 1373–1411 K for fcc-Mn). Stablilization at room temperature of unusual phases can be achieved by alloying. This is the case for Fe_xMn_{1-x} alloys whose fcc phase is stabilized over a large concentration range, $0.3<x<0.7$, and is found in an antiferromagnetic (AF) state.[4] Besides, FeMn alloys are well known as standard AF materials and are frequently used in spin-valve elaboration.[2] The fcc FeMn structure can still be stabilized by adding small amounts of Cu for $x<0.3$ and C for $x>0.7$. Such FeMn(Cu) and FeMn(C) ternary systems are also AF ordered.[4] In the Fe-rich side, binary FeMn alloys exhibit two martensitic phase transitions at room temperature. At $x=0.7$, the alloy undergoes a fcc to hcp transformation and a hcp to bcc one above $x=0.9$. The alloy remains in an AF magnetic state up to $x=0.9$ and becomes ferromagnetic (FM) at larger x values. Under a temperature increase, the fcc phase becomes stable through a hcp to fcc martensitic transformation for Fe concentrations between 0.7 and 0.9, and through a bcc to fcc transformation beyond $x=0.9$.[5]

Alternatively, new phases may be stabilized at room temperature by pseudomorphic growth of thin films on an appropriate substrate.[6] In this work, Fe_xMn_{1-x} alloy thin films and superlattices (SL's) have been synthesized on Ir(001). The existence of the fcc and bcc phases for bulk binary alloys in the Fe-rich side of the phase diagram, with lattice parameters surrounding the in-plane parameter of Ir(001), has been a motivation to prepare both phases by epitaxy using the induced anisotropic strain. In an extensive structural study, we show that FeMn thin films are strongly tetragonalized with c/a ratios between 1 (bcc structure) and $\sqrt{2}$ (fcc structure).[7] This offers the opportunity for studying magnetic properties along the so-called Bain path.[8]

Moreover, the motivation to prepare epitaxial phases is also to obtain FM states for atoms with expanded volume and to test the theoretical predictions of enhanced magnetic moments. Among $3d$-transition metals, Mn is probably the most exciting element, since the atomic Hund's rule leads to a magnetic moment of $5\mu_B$. However, in the case of fcc Mn, a large atomic volume is not a sufficient condition to obtain a high-spin FM state.[3] This leads to the necessity of growing Mn in a phase with structure as close as possible to the bcc one. Several attempts have recently been made especially by deposition of a few monolayers (ML) on top of FM

substrates[9–16] or non-FM ones.[15–19] In the case of growth on a $3d$ FM element, Mn exhibits a structural transition at an early stage of growth (above 2 ML) and later on quickly recovers its Mn-α bulk phase. For coverage below 1 ML, a net magnetic moment is usually observed with magnitude ranging from 1.6 to $4.5\mu_B$. The Mn-substrate magnetic coupling is FM for Co (Ref. 14) and Ni (Refs. 15,16) while it has been observed to be AF (Refs.11,12) or FM (Ref. 13) for Fe. For coverage above 1 or 2 ML, no ferromagnetic ordering has been evidenced and different magnetic arrangements have been proposed: either Mn forms FM sheets and the sheets align antiferromagnetically[9] or a reconstruction takes place leading to an AF (Ref. 20) or a ferrimagnetic[21] structure. The growth of Mn, deposited on Ir(111),[17] is epitaxial up to 4 ML where a structural transition is observed. Whatever the thicknesses which have been considered, no net magnetic moment has been evidenced. In the case of growth on Ir(001),[18] Mn has been observed to be constrained in a bct phase over large thicknesses, but with a weak magnetic moment. In this work, we will address the magnetic properties of Mn and Fe in FeMn alloys strained in a bct phase on an Ir(001) buffer.

Superconducting quantum interference device magnetometry measurements of the magnetic properties of Fe_xMn_{1-x} thin films[22] show a zero net magnetic moment in the temperature range $10\ \text{K} < T < 400\ \text{K}$ for $x < 0.75$. In contrast, a FM character has been evidenced for films with $x > 0.75$. However, magnetization measurements do not give access to the specific magnetic properties of each species and to their coupling. Therefore, an atom-selective probe is required to investigate the magnetic states of Fe and Mn above and below $x = 0.75$.

X-ray magnetic circular dichroism (XMCD) is the most commonly used tool to selectively investigate element-specific magnetic properties. However, there have also been significant advances in the area of x-ray resonant magnetic scattering (XRMS) using linearly[23–28] or circularly[28–35] polarized light to study $3d$ magnetic multilayers, thin films, and surfaces.

In this paper, we present a soft x-ray resonant magnetic reflectivity study performed at the $L_{2,3}$ edges of Fe and Mn on two Fe_xMn_{1-x}/Ir(001) SL's with Fe concentrations, $x = 0.7$ and 0.9, corresponding to the two different magnetic states found for FeMn alloys. Measurements on a $Fe_{0.9}Mn_{0.1}$ thin-film layer grown on an Ir(001) buffer have also been performed at both L edges. The measurements were carried out in a transverse geometry, by analogy with magneto-optic Kerr effect measurements with the goal to determine the magnetic moments carried per Fe and Mn atoms in these alloys, separately, and their relative orientations.

II. EXPERIMENTAL DETAILS

The experiments were performed using linearly polarized light at the U4B beamline at the National Synchrotron Light Source at Brookhaven National Laboratory.[36] The radiation emitted from a bending magnet source in the orbital plane of the storing ring, was used in order to get a high rate of linearly polarized light ($\approx 97\%$). The monochromator is a grating with 1200 lines per mm which allows to reach the Fe and Mn $L_{2,3}$ edges with high-energy resolution (of the order of 90 meV at the Fe edges). The intensity of the incident beam was monitored by the photocurrent from a gold mesh.

Reflectivity curves were recorded in specular condition as a function of the energy of incoming photons for a set of angles. A vacuum compatible $\theta - 2\theta$ goniometer with two vertical axes was used in a transverse $\pi - \pi$ scattering geometry.[37] An external field up to 1400 G was delivered perpendicularly to the scattering plane by a Bitter electromagnet. This magnetic field is large enough to saturate the sample as it has been checked by measuring by XRMS selective hysteresis loops. The detectors were either a proportional gas counter for the experiments performed on the superlattices, or a photodiode for those on the thin film. In both cases, the horizontal aperture was set to 1°. The experiments were performed at room temperature.

III. SAMPLE PREPARATION AND STRUCTURE

The samples are grown by molecular-beam epitaxy, in a UHV chamber, at a residual vacuum of 2.10^{-11} torr. MgO(001) single crystals are used as substrates and a 400-Å-thick Ir(001) buffer layer is first deposited on the substrate. Details on the MgO preparation and buffer elaboration are discussed in Ref. 6. Ir evaporation is obtained using electron bombardment, whereas Fe and Mn are evaporated by using Knudsen cells. The Fe_xMn_{1-x} alloys are prepared by coevaporation of the two pure metals, while monitoring their partial pressures to achieve the desired stoichiometry. In this study, we focus on two samples which have been prepared for the same nominal parameters except for the alloy stoichiometry chosen on both sides of the transition occuring at $x = 0.75$. Their structure has been investigated by anomalous x-ray diffraction,[38] grazing incidence x-ray diffraction in the symmetric mode, as well as by measurements of maps of the scattering intensity around the (111) Ir buffer peak in the asymmetric scattering condition under fixed grazing incidence. The combination of these methods allowed us to fully characterize the different superlattices. A complete report is published in a separate paper.[7] We briefly recall here the main structural characteristics of the investigated samples.

The first SL, $[Fe_{0.7}Mn_{0.3}(25.25\ \text{Å})/\text{Ir}(21.85\ \text{Å})]\times 20$ will be labeled SL70, while the second one $[Fe_{0.9}Mn_{0.1}(24.8\ \text{Å})/\text{Ir}(20\ \text{Å})]\times 20$ will be labeled SL90. SL70 exhibits a single phase with a highly coherent stacking along the growth direction. The stress induced by the Ir buffer layer propagates up to the surface. As a consequence, the $Fe_{0.7}Mn_{0.3}$ alloy exhibits a homogeneously strained body-centered-tetragonal phase (bct). The bct elementary cell is characterized by a c/a ratio of 1.22 ± 0.01 and an atomic volume of $12 \pm 0.1\ \text{Å}^3$. Elastic calculations show that the bct phase results from a deformation of the fcc bulk FeMn structure. In contrast, two different and coherent SL phases were actually identified within the SL90 sample. The first one, located near the buffer layer, is, as for SL70, a buffer-strained phase. The bct $Fe_{0.9}Mn_{0.1}$ alloy structure has a c/a ratio of 1.17 ± 0.01 and an atomic volume of $11.9 \pm 0.1\ \text{Å}^3$. The elastic calculations indicate, as previously, that this first phase in SL90 arises from the deformation of the bulk fcc $Fe_{0.9}Mn_{0.1}$ structure. The second phase is located near the surface of the sample. The stress induced by the Ir buffer has relaxed. This phase may be seen as a set of $Fe_{0.9}Mn_{0.1}$/Ir

bilayers in mutual strain. The structure of the alloy is also a bct one with a c/a ratio of 1.09 ± 0.01 and an atomic volume of 11.7 ± 0.1 Å^3. It results from the deformation of the bcc $Fe_{0.9}Mn_{0.1}$ alloy. These two phases in SL90 occur with respective proportions of the order of 37% for the strained fcc phase (SR1) and 63% for the strained bcc one (SR2).

Obviously, the existence of two different structural phases with different alloy structures in SL90 has to be taken into account when analyzing the XRMS data which average signals from both phases. In order to overcome this problem, it is necessary to separate the experimental XRMS signal into its two components originated from each structural phase. With this aim, we have grown a 30-Å $Fe_{0.9}Mn_{0.1}$ thin film (TF90) covered by a 30-Å-thick Ir capper layer, on a Ir(001) buffer, the structure of which is expected to be similar to that of the first bilayer of SL90. The structural analysis performed on this thin film confirmed that the alloy is in a single buffer-strained bct phase, with a c/a ratio of 1.19 ± 0.01 and an atomic volume of 11.9 ± 0.1 Å^3, equivalent to SR1 phase. Therefore, the XRMS results on this $Fe_{0.9}Mn_{0.1}$ thin film will be assumed to correspond to the magnetic properties of the SR1 phase.

IV. XRMS ANALYSIS

XRMS has its origin in a magnetic-sensitive contribution to the resonant atomic scattering factor appearing at characteristic atomic absorption-edge energies.[39] This sensitivity arises from the spin-orbit splitting of the core-level and the exchange splitting of the empty states involved in the transition. At the $L_{2,3}$ absorption edges of $3d$ transition metals, the resonant magnetic scattering can be derived within a dipolar approximation ($2p\rightarrow3d$ transitions) and the resonant atomic scattering factor is

$$f=-(\hat{\mathbf{e}}_f\cdot\hat{\mathbf{e}}_i)(f_0+f'-if'')-i(\hat{\mathbf{e}}_f\times\hat{\mathbf{e}}_i)\cdot\hat{\mathbf{z}}(m'-im''), \quad (1)$$

where $\hat{\mathbf{e}}_f$ and $\hat{\mathbf{e}}_i$ are the polarization vectors of the out and in-going x-ray beams, f_0 is the Thomson charge scattering amplitude, f' and f'' are the resonant terms related to the regular nonmagnetic anomalous scattering. The dependence on magnetism comes from the second term where $\hat{\mathbf{z}}$ stands for the unit vector along the magnetization direction. The imaginary part of its resonant complex amplitude m'' is equivalent to the XMCD signal,[30] m' being the real part.

The magnetic properties of the FeMn layers can be studied by measuring the scattered intensities I^+ and I^- for two opposite directions of a saturating magnetic field applied within the planes of the layers and by recording the asymmetry ratio $R=(I^+-I^-)/(I^++I^-)$ as a function of either the incident photon energy E or the scattering angle θ.[27,29]

In the transverse mode, the asymmetry ratio may be described using the kinematical approach as[40]

$$R=\frac{2\tan(2\theta)[F_iM_r-F_rM_i]}{\tan^2(2\theta)|M^2|+\{1+[1-\tau_L/(1+\tau_L)\cos^2(2\theta)]\}|F^2|}, \quad (2)$$

where τ_L is the linear polarization rate and

$$F=\sum_{\text{unit cell}}-(f_0+f'-if'')e^{iqd}=F_r-iF_i, \quad (3)$$

$$M=\sum_{\text{unit cell}}(m'-im'')e^{iqd}=M_r-iM_i, \quad (4)$$

where q is the scattering vector and d is the interplanar distance along the growth axis. This expression shows the interplay between the real and imaginary parts of the charge (F) and magnetic (M) structure factors. It allows us to reproduce the energy dependence of the asymmetry ratio measured on top of a chemical modulation Bragg peak of a multilayer, which occurs at a fixed q value.[26] However, in order to simulate the energy dependence of the asymmetry ratios, either for a multilayer or for a thin film, which are measured at θ fixed and to extract the useful information on the magnetic properties of the sample, a magneto-optical approach is required.[26,27,29] The calculation of the reflected intensities is achieved in a Fresnel formalism in the transverse geometry which takes into account the layered structure of the samples in a matrix notation. In this approach, the whole optical response of the media is contained in the dielectric tensor which is a nondiagonal Hermitian matrix. The diagonal matrix elements are related to the charge scattering factor, the off-diagonal elements being related to the magnetization-sensitive terms. They are strongly coupled in the development of the calculation. The interfacial roughness, a major ingredient in the reflectivity analysis, is taken into account by an extension of the Vidal and Vincent approach.[41] A complete description of the formalism will be published elsewhere.[42]

In the data analysis, the imaginary parts of the charge and magnetic resonant scattering factors are obtained from absorption and XMCD measurements from ''standard'' samples. Their real counterparts are derived from the Kramers-Kronig relationship. To our knowledge, no XMCD measurements have been reported on Fe_xMn_{1-x} alloys, neither on bulk samples, since they are are AF ordered, nor on thin films. Therefore, for iron, we used XMCD data which have been collected on a bcc Fe thin film, where the application of the sum rules yields $M_{\text{Fe}}^{3d}=2.1\mu_B$,[43] a value nearly identical to that of bulk Fe. For manganese, the choice of a ''standard'' sample showing magnetic ordering is not straightforward. Bulk manganese is AF ordered and hence no XMCD is observable. A few studies have been dedicated to Mn overlayers on magnetic $3d$ substrates where a XMCD signal has been observed.[11–16] If the oxydation of the Mn thin film is avoided, the shape of the $L_{2,3}$ absorption spectra is comparable to that of metallic Mn.[44] However, it is known that the branching ratio defined as $I(L_3)/[I(L_3)+I(L_2)]$ decreases with the magnetic moment of Mn.[17] In most cases where XMCD has been observed at the Mn $L_{2,3}$ edges, for Mn on Co(001),[14] Mn on Ni,[15] and Mn on Fe,[12,13] the line shapes and the branching ratios looked very much the same. Consequently, in this study, we used absorption and XMCD data from measurements carried out in a nearly oxygen-free environment on a Mn monolayer deposited on Fe(001).[44] In that case, Mn is found to grow in a bct structure ($c/a=1.06$) and shows a net magnetic moment ferromagnetically coupled with the Fe one. Its amplitude has been estimated to

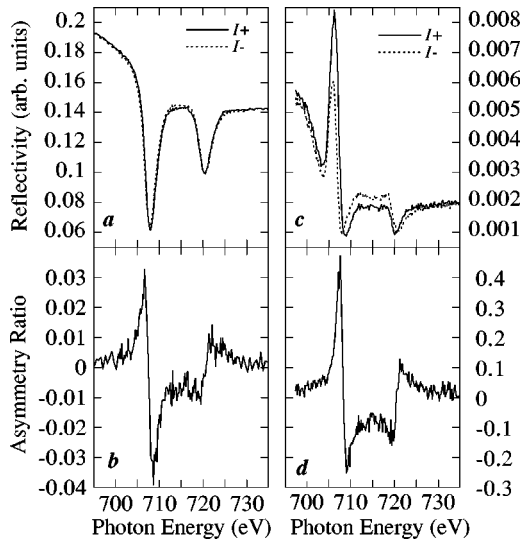

FIG. 1. Energy dependence of the reflectivity measured at the Fe $L_{2,3}$ absorption edges and at $\theta=15°$ for two opposite orientations of the applied magnetic field (top panels) and energy dependence of the magnetic asymmetry ratio (bottom panels) for SL70 (a,b) and SL90 (c,d).

be $M_{\mathrm{Mn}}^{3d}=3\mu_B$ from the comparison between the experimental amplitude and the calculated one for an isolated Mn^{2+} ion.[13,44] The use of these resonant parameters in the XRMS calculations implies *a priori* two assumptions: (i) the shape of the energy dependence of f'' and m'' at the $L_{2,3}$ edges of Fe and Mn is assumed not to be significantly affected by a change in the crystal structure, and (ii), the amplitude of the XMCD signal is proportional to the atomic magnetic moment. From the later, the factor scaling the m' and m'' values used in the simulation of the asymmetry ratios can be used to derive the value of the magnetic moment from its value in the reference sample. This procedure, which has also been employed in a XMCD study of Fe/Cr multilayers,[45] allows us to determine the values M_{Fe}^{3d} and M_{Mn}^{3d} of the magnetic moment in our samples from the references. The accuracy of the determination relies on the accuracy of the XMCD data analysis.

V. EXPERIMENTAL RESULTS

A. XRMS at the Fe $L_{2,3}$ edges

Figure 1 shows the energy-dependent reflectivity curves (top panels) measured for two opposite directions of the applied magnetic field at the Fe $L_{2,3}$ edges at an incident angle $\theta=15°$ for SL70 [Fig. 1(a)] and SL90 [Fig. 1(c)]. The corresponding XRMS asymmetry ratios R are exhibited in the bottom panels of Fig. 1. The strong resonances, observed in the reflectivity curves around 708 and 720 eV correspond to the L_3 and L_2 edges, respectively. The whole energy dependence is quite different for both samples especially at the L_3 edge. This arises from small differences in structural parameters for both SL, demonstrating the structural sensitivity of resonant soft x-ray reflectivity measurements. The energy splitting and the amplitude difference between I^+ and I^- are much more pronounced in SL90, which indicates that Fe atoms in this sample carry a stronger magnetic moment. Surprisingly, although the energy dependences of the reflectivity are rather different, those of the two R's are quite similar. However, their amplitude shows a large difference in line with the amplitude of the changes induced by the flipping of the applied magnetic field in the reflectivity. While SL90 gives rise to a strong R maximum value of about 40% at $E=707.5$ eV, the maximum value for SL70 only reaches 3%, at the same energy. In order to understand these results in terms of magnetic moment variation, it is required to simulate both asymmetry ratios since, at variance with XMCD, the amplitude of R is not simply linked to the magnetic moment amplitude.

The simulation of R as a function of the photon energy for both superlattices has been performed considering a homogeneous alloy and assuming that all the Fe atoms carry the same magnetic moment. Even though soft x rays are used in the vicinity of the Fe $L_{2,3}$ edges where absorption is strong, the whole thickness of the SL's, which is about 900 Å, is probed as ascertained by the observation of Kiessig fringes on each side of the chemical modulation Bragg peak, in a $\theta/2\theta$ scan. However, these fringes disappear in a small energy range, from 706 to 709 eV around the energy of the maximum of the white line (707.3 eV). This implies that, for this 3 eV window, the near-buffer phase of SL90 is not entirely probed by the x rays and that part of the Fe magnetic moments in this phase do not participate in the asymmetry ratio. Our calculation, using the optical approach, fully takes into account the absorption correction through the dielectric tensor. Therefore, within that tiny energy window, the value of the average magnetic moment may change since the magnetic moment of Fe atoms in SR1 and SR2 are not weighted in the same way, which could imply some discrepancies between experiment and calculation.

The structural parameters required in the optical approach are the thicknesses and the densities of the layers, as well as the roughnesses (σ) at the different kinds of interfaces. The first two parameters derive from the structural investigation (refer to Sec. III and to Ref. 7). The roughnesses have been determined from the analysis of the specular x-ray reflectivity. In the case of the SL's, their values were determined by

TABLE I. Structural parameters used in the optical approach for the calculations of the reflectivity for the three samples under investigation.

	$t_{\mathrm{Ir\ buffer}}$ (Å)	$\sigma_{\mathrm{Ir\ buffer}}$ (Å)	$\rho_{\mathrm{Ir\ buffer}}$ (10^{-28} atoms m^{-3})	t_{FeMn} (Å)	σ_{FeMn} (Å)	ρ_{FeMn} (10^{-28} atoms m^{-3})	t_{Ir} (Å)	σIr (Å)	ρ_{Ir} (10^{-28} atoms m^{-3})
SL70	400	1	7.06	25.3	3	8.31	21.8	3	7.21
SL90	400	1	7.06	24.9	2.2−8.5	8.49	19.9	2.2−8.5	6.99
TF90	335±1	1±0.1	7.06	31±2	2.3±0.1	8.43	32±2	1.4±0.1	7.06

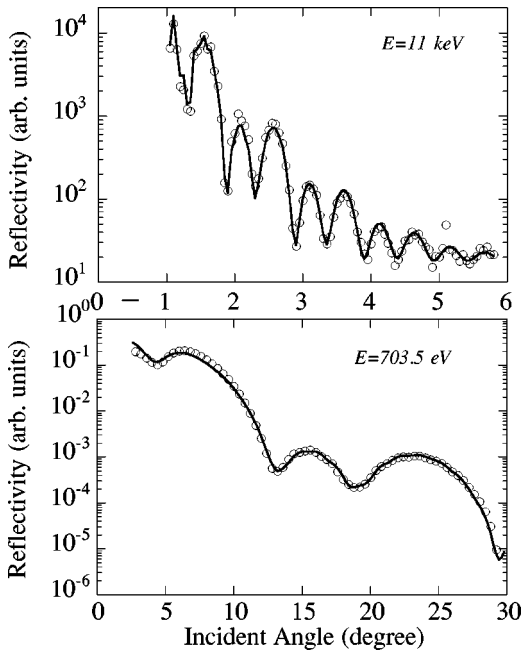

FIG. 2. Angular dependence of the reflectivity (open circles) measured at 11 keV (top panel) and at 703.5 eV (bottom panel) together with the best calculations (solid line).

Fischer[22] using a calculation which allows one to introduce a gradient of interfacial roughnesses from the bottom to the top of the SL. For the TF90 sandwich, the structural parameters are determined from the refinement of the reflectivity curves measured at 11 keV (Fig. 2) using the SPUR package.[46] The structural parameters are given in Table I and were kept fixed in the calculations of the different asymmetry ratio. The only free parameter is a scaling factor affecting the magnitude of the ''standard'' XMCD used in the calculation of the atomic magnetic scattering factor, in order to adjust the value of the magnetic moment.

Figure 3 compares the experimental and calculated R curves at $\theta=15°$ for SL70. The calculated ones were obtained by using two different values for the Fe magnetic moment. The left panel displays the curve obtained using the ''standard'' $M_{\mathrm{Fe}}^{3d}=2.1\mu_B$/atom value for bcc Fe, whereas in the right panel the Fe magnetic moment has been reduced by a scaling factor of 0.13, leading to a value $M_{\mathrm{Fe(SL70)}}^{3d}=0.27\mu_B$ which enables us to fit the experimental curve.

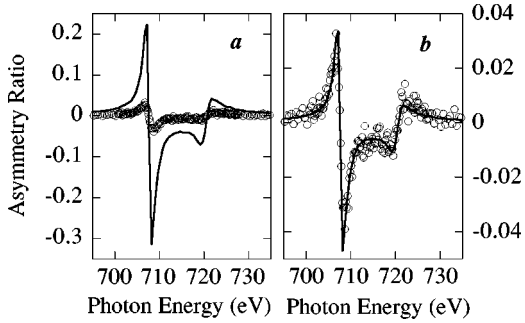

FIG. 3. Experimental (open circles) and calculated (solid line) asymmetry ratios obtained for the SL70 superlattice, for $\theta=15°$ at the Fe $L_{2,3}$ absorption edges: (a) the calculated curve has been obtained assuming $M_{\mathrm{Fe}}=2.1\mu_B$/atom, (b) same as (a) but for $M_{\mathrm{Fe}}=0.27\mu_B$/atom.

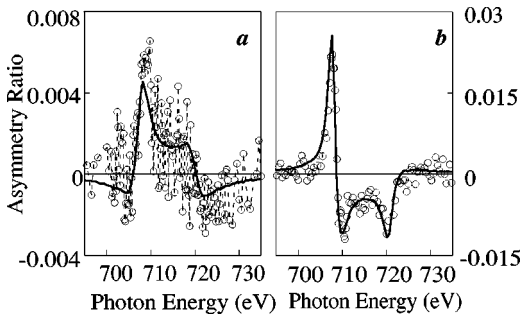

FIG. 4. Experimental (open circles) and calculated (solid line) asymmetry ratios obtained for the SL70 sample, for $\theta=7°$ (a) and $\theta=13°$ (b), at the Fe $L_{2,3}$ absorption edges assuming $M_{\mathrm{Fe}}=0.27\mu_B$/atom.

This strongly reduced magnetic moment of Fe atoms in SL70 does not only allow us to describe the experimental asymmetry ratio recorded at $\theta=15°$, but also those recorded at other angles, as for instance, at $\theta=7°$ and 13° (Fig. 4). The decrease of the signal-to-noise ratio with decreasing θ is related to the $\tan(2\theta)$ angular dependence of R when measured with linearly polarized photons [Eq. (2)]. Because of the q dependence of R spectra through the magnetic and charge structure factor, the energy dependence of the R's changes with the value of the incident angle. In particular, the R spectrum measured at $\theta=7°$ is different with respect to the others. A very good agreement between calculated and experimental data is found for the three scattering angles. These results allow us to determine that Fe atoms in SL70 carry a weak magnetic moment of $0.27\pm0.05\mu_B$/atom.

Figure 5 displays experimental and calculated R curves obtained for the SL90 sample at $\theta=10°$ [Fig. 5(a)] and 15° [Fig. 5(b)] at the Fe $L_{2,3}$ absorption edges. The fitting of both R spectra has been obtained by using the XMCD data, without any scaling factor. Therefore, we deduce a $3d$ Fe magnetic moment of $2.1\pm0.05\mu_B$/atom for SL90. As is mentioned in Sec. III, SL90 exhibits two $Fe_{0.9}Mn_{0.1}$ phases and the R spectra result from averaging their contribution over the whole sample. The $2.1\mu_B$/atom value, thus corresponds to a mean atomic magnetic moment averaged over the two phases. In order to separately evaluate the Fe magnetic moment in both phases, we performed another XRMS measurement on the single-phase $Fe_{0.9}Mn_{0.1}$ thin film, TF90, described in Sec. III. This should give a selective measurement of the Fe magnetic moment for the near-buffer phase in the SL90 sample.

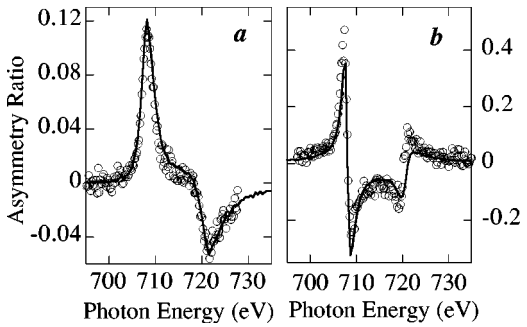

FIG. 5. Experimental (open circles) and calculated (solid line) asymmetry ratios obtained for the SL90 sample, for $\theta=10°$ (a) and $\theta=15°$ (b), at the Fe $L_{2,3}$ absorption edges with $M_{\mathrm{Fe}}=2.1\mu_B$/atom.

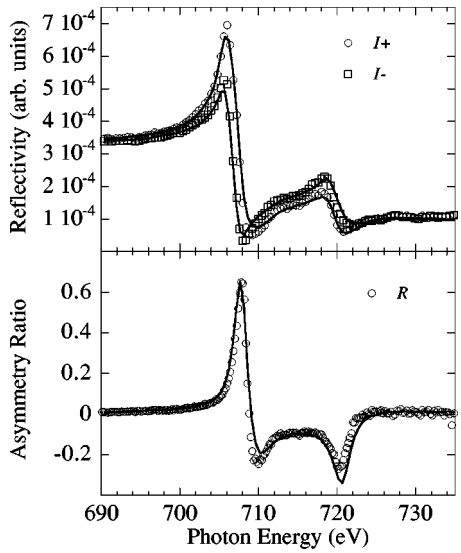

FIG. 6. Top panel: Energy dependence of the reflectivity measured on a $Fe_{0.9}Mn_{0.1}$ thin film at the Fe $L_{2,3}$ absorption edges for two opposite orientations of the applied magnetic field at $\theta = 26°$, and the best calculations (solid lines) with $M_{Fe} = 2.1\mu_B$/atom. Bottom panel: derived experimental (open circles) and calculated (solid line) asymmetry ratios.

Figure 6 shows the energy dependence of the reflectivity at $\theta = 26°$ for two opposite directions of the applied magnetic field (upper panel) and the asymmetry ratio (bottom panel) measured for TF90 at the Fe $L_{2,3}$ edges, as well as their simulation. The calculations have been carried out using the structural parameters given in Table I and a magnetic moment for the Fe atoms $M_{Fe}^{3d} = 2.1\mu_B$/atom. Here, we show that the energy dependence of the reflectivity may be quite nicely reproduced and again a good agreement is found between experimental and calculated R's. As the M_{Fe}^{3d} value found in a single phase system is identical, within the accuracy of the fitting, to the average value over the two phases in SL90, we deduce that Fe atoms do carry the same magnetic moment $M_{Fe}^{3d} = 2.1 \pm 0.1\mu_B$/atom in both distinct phases.

In conclusion, XRMS experiments at the Fe $L_{2,3}$ edge, performed on Fe_xMn_{1-x}/Ir SL's of tetragonal symmetry, yield a Fe magnetic atomic moment of $0.27 \pm 0.05\mu_B$ in the single phase SL70 and of $2.1 \pm 0.05\mu_B$ in both phases of SL90.

B. XRMS at the Mn $L_{2,3}$ edges

In this section, we present resonant magnetic reflectivity experiments performed at the Mn $L_{2,3}$ absorption edges. Two important questions dealing with the magnetism of Mn in strained FeMn thin-film alloys can be addressed: first, do the Mn atoms carry a net magnetic moment and second if so, how is it coupled to the Fe one? In order to answer these questions, we focused our study on the $Fe_{0.9}Mn_{0.1}$ thin film where Mn atoms are diluted in a high-spin matrix. We have to mention that experiments performed on SL70 and SL90 did not evidence a magnetic asymmetry at the Mn $L_{2,3}$ edges. This has been ascribed to the level of noise in the signal which was too high at the time of the experiment, preventing the observation of an eventual low asymmetry ratio.

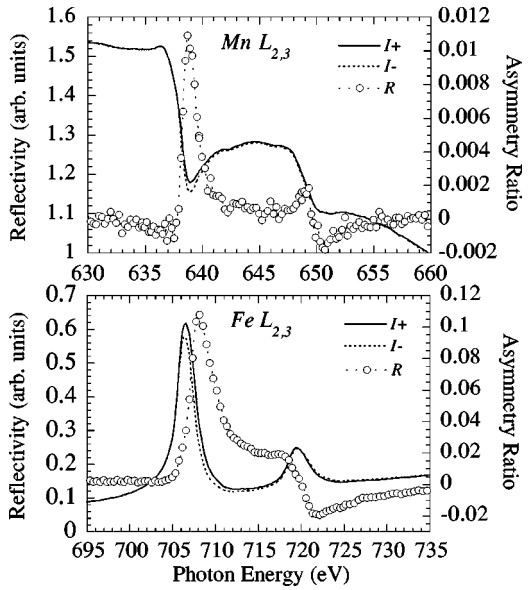

FIG. 7. Energy dependence of the reflectivity measured on a $Fe_{0.9}Mn_{0.1}$ thin film at $\theta° = 20$ for opposite orientations of the applied magnetic field at the Mn $L_{2,3}$ absorption edges (top panels) and at the Fe $L_{2,3}$ absorption edges (bottom panels). The asymmetry ratios (open symbol) are also reported, the dashed line being just a guide for the eyes.

Figure 7(a) shows the energy dependences of the reflectivity together with the weak R spectrum recorded on TF90 at the Mn $L_{2,3}$ edges at an incident angle $\theta = 20°$. Magnetic resonances are clearly visible at the Mn L_3 and L_2 edges. A derivative shape occurs at the Mn L_2 edge. The observation of a nonzero magnetic signal evidences the existence of a net magnetic moment carried by the Mn atoms in this $Fe_{0.9}Mn_{0.1}$ thin film. At the maximum, R is about 0.011 ± 0.001. We note that noise in the R curve is considerably reduced compared to noise in Fig. 4(a), while the R values are similar. This is due to changing the proportional gas counter for a photodiode. Figure 7(b) exhibits the reflectivity and the R spectrum obtained on TF90 at the Fe $L_{2,3}$ edges at an incident angle $\theta = 20°$.

It is important to stress that, even though the Fe [Fig. 7(b)] and Mn [Fig. 7(a)] asymmetry ratios, measured in the same conditions ($\theta = 20°$), have the same spectral shape with the same sign, we cannot conclude on a ferromagnetic coupling of both species. At variance with XMCD, where the nature of the coupling would be directly determined from the relative sign of the signals,[11–13] the dichroic effect exhibited in the reflectivity are not only due to the imaginary part of the magnetic dielectric constant but also to its real part as shown in Eq. (2). The mixing of the two components is weighted by the real and imaginary parts of the structure factor which are q dependent. Therefore, even for a given element, the sign of the R curve may change with q or θ, as shown in Fig. 4. Moreover, it is worth noting that the energy dependences of the reflectivity shows an opposite behavior at the Fe and Mn edges [Figs. 7(a) and 7(b)]. At the energies of the L_3 and L_2 resonances, the Mn reflectivity exhibits dips, whereas the Fe one shows peaks. Therefore, to conclude about the relative orientations of the moments of two magnetic species, the calculation of the magnetic asymmetry ratios is required.

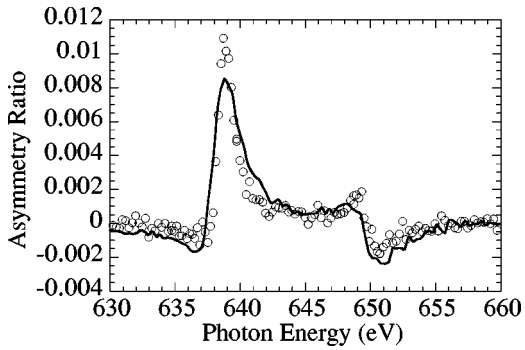

FIG. 8. Experimental (open symbols) and calculated (solid line) asymmetry ratios obtained for a $Fe_{0.9}Mn_{0.1}$ thin film, for $\theta° = 20$, at the Mn $L_{2,3}$ absorption edges assuming $M_{Mn} = 1.7\mu_B$/atom antiferromagnetically coupled to M_{Fe}.

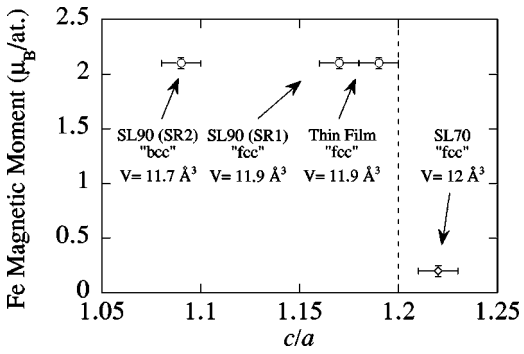

FIG. 9. Evolution of the Fe magnetic moments in Fe_xMn_{1-x} alloys as a function of the c/a ratio of the bct structure. The SL70 superlattice is shown by a diamond while the phases for SL90 are depicted by a circle. The atomic unit-cell volumes and the hypothetical unconstrained structures are indicated for each sample. The vertical dashed line at $c/a = 1.2$ indicates the critical value at which a magnetic transition is predicted to occur from Ref. 48.

Figure 8 displays the result of the calculation at the Mn edges. The solid line is obtained using the same structural parameters as those used for the calculations at the Fe edges (Fig. 6). The resonant charge and magnetic scattering factors are discussed in Sec. IV. The best agreement between experimental and calculated R spectra is obtained by applying a scaling factor of -0.57. Then the amplitude of the averaged magnetic moment is $M_{Mn}^{3d} = -1.7 \pm 0.2\mu_B$/atom, where the minus sign indicates that the Mn net magnetic moment is antiparallel to the Fe one.

In the following, we discuss the effects of uncertainties in the determination of the roughness on the sign and amplitude of the Mn magnetic moment. The influence of the value of the interfacial roughness, which is known to be a crucial parameter,[26,42] has been evaluated by calculating R spectra for different values of the roughness. It turns out that calculations performed assuming perfect interfaces ($\sigma = 0$) to compare to the values in Table I yield the same sign and an amplitude value 10% lower, within the error bars. However, if the roughness of the surface of the Ir capper is increased from 1.4 to 5 Å, while the roughnesses of the other interfaces are kept constant, a strong change is observed in the amplitude of R which leads to a value of the magnetic moment lower by 50%. A further increase of this surface roughness progressively changes the shape of the energy dependence of R as well as that of the reflectivity curve. In the same way, if the roughness of the FeMn-Ir capper interface is increased from 2.3 to 5 Å, the other roughness values being not changed, the small negative structure at 637 eV is enhanced leading to a derivative shape for the resonance at the L_3 edge and a positive peak replaces the derivative shape at the L_2 edge. An opposite trend occurs when only the Ir buffer-FeMn interface roughness is increased. These trials clearly show that a careful determination of the interface roughness is required. This is also true for the determination of the thicknesses of the magnetic and capper layer especially when they are very close. With that aim, we performed a refinement of the angular reflectivity measured in the soft x-ray range at 703.5 eV. This corresponds to a determination of the structural parameters, independent of the refinement performed at 11 keV. The best fit is shown in the bottom panel of Fig. 2. The values of the thicknesses, of the densities, and of the roughnesses fall within the error bars of the values determined from the fit of the hard x-ray reflectivity which are given in Table I. This gives strong support for the values of the parameters used in the calculation and make us confident in the validity of the determination of the Mn moment value from the fitting of the asymmetry ratios at the Mn $L_{2,3}$ edges. Our XRMS measurement allows us to conclude that Mn atoms, in a bct ($c/a = 1.18$) $Fe_{0.9}Mn_{0.1}$ thin film, bear a net magnetic moment of $1.7\mu_B$, on average, antiferromagnetically coupled with the Fe ones.

Two possible arrangements of the Mn subsystem could give rise to the observed signal at the Mn edge: a ferromagnetic one with every Mn atom carrying the same magnetic moment $M_{Mn} \approx 1.7\mu_B$ and oriented antiparallel to the ferromagnetically ordered Fe $2.1\mu_B$ first-neighbor magnetic moments, or an uncompensated antiferromagnetic arrangement of the Mn subsystem itself. Actually, such a system has theoretically been predicted for 1 and 2 Mn monolayers on Fe(001) with a bct structure.[21] In a homogeneous $Fe_{0.9}Mn_{0.1}$ alloy, the second possibility is, however, quite unlikely to occur. The number of Mn-Fe first-neighbor pairs is about one order of magnitude larger than that of Mn-Mn ones, implying that the Mn-Mn magnetic interactions are very few and cannot lead to a magnetic arrangement comparable to that of a monolayer. We thus think that Mn-Fe magnetic interactions are responsible for the global arrangement of the Mn subsystem. Although the possibility of a nonhomogeneous Fe-Mn alloy, due to a superficial segregation of Mn atoms for instance, cannot be fully ruled out, its effect should be very small since such an effect leads to small deviations of the Mn concentration from the mean value averaged through the layer.[47] This is also supported by the observation that the species selective reflectivity measurements can be quantitatively simulated using a homogeneous model. We, therefore, conclude that each Mn atom in the $Fe_{0.9}Mn_{0.1}$ alloy carries a magnetic moment of the order of $\approx 1.7\mu_B$.

VI. DISCUSSION

XRMS experiments performed at the Fe $L_{2,3}$ absorption edges enabled us to determine the values of the magnetic moment carried by Fe atoms in the different bct phases of buried FeMn thin-film alloys. The structural and magnetic

findings are summarized in Fig. 9, where the amplitudes of the Fe magnetic moments in each phase are plotted as a function of the c/a ratio of the cristallographic parameters describing the alloy structure. The values of the atomic volume of the elementary cell, as well as the phase which the FeMn layers would have if they were unconstrained, are also indicated in Fig. 9. The main result is that Fe atoms in $Fe_{0.9}Mn_{0.1}$ samples are in a high-spin (HS) FM state, whereas in the $Fe_{0.7}Mn_{0.3}$ sample they are in a low-spin (LS) FM state.

The growth of $Fe_{0.9}Mn_{0.1}$ alloys in the SL90 superlattice has given rise to the formation of two phases which, respectively, originate from the deformation of the fcc and bcc structures existing in bulk Fe_xMn_{1-x} for $x=0.9$.[4,5] This is interesting since it allows us to study the influence of the structure on the magnetic properties for the same Fe and Mn concentrations in the alloy. As the bulk bcc $Fe_{0.9}Mn_{0.1}$ alloy is FM ordered and the fcc one is AF, different magnetic states would be expected for the two phases of sample SL90. However, surprisingly, we found that both phases have the same HS FM behavior. In fact, these results can be understood by regarding the magnetic properties of the Fe atoms as a function of the c/a ratio of the elementary cell. This ratio enables us to describe the tetragonalization level of the bct structure which varies from $c/a=1$ for a bcc structure to $c/a=\sqrt{2}$ for a fcc one. We have shown that Fe atoms carry a HS moment in the two phases of SL90 and in the $Fe_{0.9}Mn_{0.1}$ thin film (of $\approx 2.1\mu_B$ per atom as bulk bcc Fe) until at least $c/a<1.2$. This observation is consistent with the results of theoretical studies performed by Krasko and Olson on bct Fe.[48] Within a Stoner-model approach, they have found that going along the Bain path from bcc to fcc, the Fe FM phase is first stable, up to $c/a=1.2$. Beyond that a transition occurs and the NM phase is stable at higher c/a values. However, one should point out that the authors did not consider the magnetic AF state which is that of the bulk fcc FeMn systems.[4,5]

In the case of SL70, Fe atoms are found in a FM state and carry a low magnetic moment about $\approx 0.27\mu_B$ per atom. This LS FM state is a magnetic phase since bulk $Fe_{0.7}Mn_{0.3}$ alloys are AF ordered. Its existence might be correlated to the strong tetragonal distortion, $c/a=1.22$, which deviates this artificial FeMn phase far from the stable AF fcc bulk phase.

It is worth observing that in Fe/Ir(001) superlattices, corresponding to $x=1$, a magnetic transition has also been observed (at 4 K) from a NM (or AF) state to a HS one when going through the Bain's path from the fcc structure to the bcc one, with an intermediate LS state which occurs at a very similar c/a value of 1.24–1.25.[6] This shows that the Mn concentration does not play a direct part in the change of the magnetic properties. However, it does play a part in the increase of the tetragonalization induced by the Ir substrate, since the c/a parameter varies from 1.17 in SR1 to 1.22 in SL70 and 1.3 a Mn/Ir multilayer.[22] It probably does also play a part in the amplitude of the reduction of the magnetic moment.[49]

All these results on FeMn alloys with $x\geqslant 0.7$ strongly support the existence of a transition in Fe between the ferromagnetic HS state of the bcc structure to a NM (or AF) state at around $c/a=1.2$, consistently with Krasko and Olson's predictions.

Let us mention that, in all the samples of the present study, the atomic volume is less than 12 Å^3, and lower than the volume for which the transition between a NM to a FM behavior is predicted for fcc Fe ($V=12.34$ Å^3).[3] In this study, we show that, in a strain bct $Fe_{0.9}Mn_{0.1}$ alloy thin film whose hypothetical unconstrained phase is fcc, a HS FM state may exist with a small atomic volume (11.9 Å^3) through the tetragonalization of the fcc structure.

We next turn to the discussion of the magnetic properties of Mn. In the bct $Fe_{0.9}Mn_{0.1}$ thin film ($c/a=1.18$), the Mn magnetic moment is found to be antiferromagnetically aligned with the Fe one and its amplitude is about $1.7\mu_B$/atom. This AF coupling is opposite to most of the available experimental results, derived from neutron scattering, on Mn diluted in Fe. A parallel coupling has been obtained, with different values of the Mn moment, ranging from $0.77\mu_B$ (Ref. 50) to $1\mu_B$.[51] Nevertheless, an antiparallel ($-0.82\mu_B$) orientation of a Mn moment has also been found,[52] as well as a null Mn moment.[53] We stress that our measurements are species selective. In that sense, it is a more direct probe of the Mn magnetism than neutron-scattering measurements are. Even though the uncertainty on the determination of the magnetic moment amplitude is closely related to the uncertainty in the value of the Mn moment derived from XMCD analysis,[44] and so could be large, the antiparallel orientation of the Mn moment relative to the Fe one is unquestionable. Nevertheless, we cannot exclude that the magnetic Mn state can be very sensitive to the sample preparation, leading to the different observed behaviors.

Actually, Mn is a very critical case as reported in several calculations concerning the electronic structure and magnetic properties of $3d$ impurities in ferromagnetic iron.[54–56] Our result is in good agreement with the calculations of Akai *et al.*[54] who found a Mn magnetic moment of $-1.7\mu_B$/atom and with a more recent result of Paduani *et al.* who found for an isolated Mn atom in a Fe matrix a magnetic moment of $-1.1\mu_B$/atom.[49] However, it strongly disagrees with the calculations of Drittler *et al.*[56] which give a Fe-Mn ferromagnetic coupling with a Mn magnetic moment of about $0.7\mu_B$. The explanation for these contradictory theoretical results can be found in the dependence of the magnetic moment M of a $3d$ impurity in iron on the atomic number Z. The calculated variation of M exhibits a sharp transition from negative (AF coupling) to positive (FM coupling) values around $Z=25$ (Mn atomic number) with increasing Z values.[54,56] Depending on approximations in the calculation, such as the exchange-correlation potential or the angular momentum cutoff, this transition may be found to occur at values larger or smaller than $Z=25$.[56] Both coupling situations can even be found to be stable for Mn in bcc or in fcc Fe, as has been shown by Anisimov.[55]

In any case, we know that the structure of $Fe_{0.9}Mn_{0.1}$ is strongly tetragonalized ($c/a=1.18$), which induces a symmetry reduction and, therefore, a change in the hybridization between the $3d$ states of the impurity and those of the matrix element. Our result thus indicates that the c/a value is a pertinent parameter which should be taken into account in the theoretical calculations and influences the Z value of the transition.

VII. CONCLUSION

Thin films of Fe_xMn_{1-x} alloys, in the range $x \geqslant 0.7$, with a centered tetragonal structure, have been investigated by linearly polarized soft x-ray resonant magnetic reflectivity. Taking advantage of the atomic selectivity of the method, we have been able to measure the Fe magnetic moments in the different phases found. We showed that the drastic reduction of the Fe magnetic moment between $x=0.9$ and $x=0.7$ mainly depends on the value of the c/a ratio, a and c being the structural parameters in the bct structure. The change of behavior between HS to LS occurs around a c/a value of 1.2, close to the one theoretically predicted for bct Fe (Ref. 48) and experimentally found in Fe/Ir(001) superlattices.[6] These experimental results allow us to discuss magnetic properties of Fe alloyed with Mn, when going through the Bain's deformation path, at least for $x \geqslant 0.7$. Moreover, our XRMS measurement allows us to conclude that Mn atoms, in a bct ($c/a=1.18$) $Fe_{0.9}Mn_{0.1}$ thin film, bear a net magnetic moment of $1.7\mu_B$, antiferromagnetically coupled with the Fe ones. We are presently investigating the Mn magnetic moment when going through the Bain's deformation path for $x \geqslant 0.7$.

On another hand, this work also illustrates that soft x-ray resonant magnetic reflectivity in the transverse mode is a powerful element-specific magnetometry method when combined with a proper computational formalism allowing its quantitative simulation. We have shown that it is possible to analyze small changes in the energy-dependent reflectivity and to extract weak values of the magnetic moments (here $0.3\mu_B$) in a thin buried layer. It is of special interest for films containing several magnetic elements because of its species selectivity. Finally, the data are recorded in a very simple specular scattering geometry. Therefore, this technique appears to be promising for future investigations of very thin films, either amorphous or crystalline.

ACKNOWLEDGMENTS

We wish to thank the staff of the NSLS facility at Brookhaven for the efficient assistance during the experiments. C.T. Chen and S. Andrieu are acknowledged for having provided the XMCD data used in the calculations. F.B. acknowledges a Marie Curie Research grant from the EEC.

[1] For a review, see, *Ultrathin Magnetic Structures*, edited by B. Heinrich and J. A. C. Bland (Springer-Verlag, Berlin, 1994).
[2] S.S.P. Parkin, IBM J. Res. Dev. **42**, 3 (1999).
[3] V.L. Moruzzi, P.M. Marcus, and J. Kübler, Phys. Rev. B **39**, 6957 (1989).
[4] Y. Endoh and Y. Ishikawa, J. Phys. Soc. Jpn. **30**, 1614 (1971).
[5] M. Acet, T. Schneider, B. Gehrmann, and E.F. Wassermann, J. Phys. IV **C8**, 379 (1995).
[6] S. Andrieu, F. Lahatra-Razafindramisa, E. Snoeck, H. Renevier, A. Barbara, J.M. Tonnerre, M. Brunel, and M. Piecuch, Phys. Rev. B **52**, 9938 (1995).
[7] A. Déchelette, M.C. Saint-Lager, J.M. Tonnerre, G. Patrat, D. Raoux, H. Fischer, S. Andrieu, and M. Piecuch, preceding paper, Phys. Rev. B **60**, 6623 (1999).
[8] E.C. Bain, Trans. Am. Inst. Min. Metall. Pet. Eng. **70**, 25 (1924).
[9] T.G. Walker and H. Hopster, Phys. Rev. B **48**, 3563 (1993).
[10] C. Roth, T. Kleemann, F.U. Hillebrecht, and E. Kisker, Phys. Rev. B **52**, R15 691 (1995).
[11] J. Dresselhaus, D. Spanke, F.U. Hillbrecht, E. Kisker, G. Van der Laan, J. Goedkoop, and N.B. Brookes, Phys. Rev. B **56**, 5461 (1997).
[12] O. Rader, W. Gudat, D. Schmitz, C. Carbone, and W. Eberhardt, Phys. Rev. B **56**, 5053 (1997).
[13] S. Andrieu, M. Finazzi, Ph. Bauer, H. Fischer, P. Lefevre, A. Traverse, K. Hricovini, G. Krill, and M. Piecuch, Phys. Rev. B **57**, 1985 (1998).
[14] W.L. O'Brien and B.P. Tonner, Phys. Rev. B **50**, 2963 (1994).
[15] W.L. O'Brien and B.P. Tonner, Phys. Rev. B **51**, 617 (1995).
[16] H.A. Dürr, G. van der Laan, D. Spanke, F.U. Hillbrecht, and N.B. Brookes, Phys. Rev. B **56**, 8156 (1997).
[17] W.L. O'Brien and B.P. Tonner, J. Vac. Sci. Technol. A **13**, 1544 (1995).
[18] S. Andrieu, H. Fischer, A. Traverse, and M. Piecuch, Phys. Rev. B **54**, 2822 (1996).
[19] Ch. Ross, B. Schirmer, M. Wuttig, Y. Gauthier, G. Bihlmayer, and S. Blügel, Phys. Rev. B **57**, 2607 (1998).
[20] Ruqian Wu and A.J. Freeman, Phys. Rev. B **51**, 17 131 (1995).
[21] O. Elmouhssine, G. Moraitis, J.C. Parlebas, and C. Demangeat, Phys. Rev. B **55**, R7410 (1997).
[22] H. Fischer, Ph.D. thesis, Université Henry Poincaré-Nancy I, France, 1995.
[23] C.C. Kao, J.B. Hastings, E.D. Johnson, D.P. Siddons, G.C. Smith, and G.A. Prinz, Phys. Rev. Lett. **65**, 373 (1990).
[24] J.M. Tonnerre, L. Sève, D. Raoux, B. Rodmacq, M. de Santis, P. Troussel, J.M. Brot, V. Chakarian, C.C. Kao, E.D. Johnson, and C.T. Chen, Nucl. Instrum. Methods Phys. Res. B **97**, 444 (1995).
[25] L. Sève, J.M. Tonnerre, D. Raoux, J.F. Bobo, M. Piecuch, M. de Santis, P. Troussel, J.M. Brot, V. Chakarian, C.C. Kao, and C.T. Chen, J. Magn. Magn. Mater. **148**, 64 (1995).
[26] L. Sève, Ph.D. thesis, Université Joseph Fourier, Grenoble, France, 1997.
[27] J.M. Tonnerre, L. Sève, A. Barbara-Déchelette, F. Bartolomé, D. Raoux, V. Chakarian, C.C. Kao, H. Fischer, S. Andrieu, and O. Fruchart, J. Appl. Phys. **83**, 6293 (1998).
[28] M. Sacchi and A. Mirone, Phys. Rev. B **57**, 8408 (1998).
[29] C.C. Kao, C.T. Chen, E.D. Johnson, J.B. Hastings, H.J. Lin, G.H. Ho, G. Meigs, J.M. Brot, S.L. Hulbert, Y.U. Idzerda, and C. Vettier, Phys. Rev. B **50**, 9599 (1994).
[30] J.M. Tonnerre, L. Sève, D. Raoux, G. Soullié, B. Rodmacq, and P. Wolfers, Phys. Rev. Lett. **75**, 740 (1995).
[31] J.F. MacKay, C. Teichert, D.E. Savage, and M.G. Lagally, Phys. Rev. Lett. **77**, 3925 (1996).
[32] V. Chakarian, Y.U. Idzerda, C.C. Kao, and C.T. Chen, J. Magn. Magn. Mater. **165**, 52 (1997).
[33] Y.U. Idzerda, V. Chakarian, and J. Freeland, Synch. Radiat. News. **10**, 6 (1997).
[34] J.W. Freeland, V. Chakarian, K. Bussmann, Y.U. Idzerda, H. Wende, and C.C. Kao, J. Appl. Phys. **83**, 6290 (1998).

[35] L. Sève, N. Jaouen, J. M. Tonnerre, D. Raoux, F. Bartolomé, M. Arend, W. Felsch, A. Rogalev, J. Goulon, and J. F. Bérar (unpublished).
[36] C.T. Chen, Nucl. Instrum. Methods Phys. Res. A **256**, 595 (1987); C.T. Chen and F. Sette, Rev. Sci. Instrum. **60**, 1616 (1989); C.T. Chen, *ibid.* **63**, 1229 (1992).
[37] E.D. Johnson, C.C. Kao, and J.B. Hastings, Rev. Sci. Instrum. **63**, 1443 (1992).
[38] A. Déchelette-Barbara, J.M. Tonnerre, M.C. Saint-Lager, D. Raoux, S. Andrieu, M. Piecuch, E. Elkaïm, and J.P. Lauriat, J. Magn. Magn. Mater. **156**, 111 (1996).
[39] J.P. Hannon, G.T. Trammel, M. Blume, and D. Gibbs, Phys. Rev. Lett. **61**, 1245 (1988).
[40] F. de Bergevin, M. Brunel, R.M. Galera, C. Vettier, E. Elkaïm, M. Bessière, and S. Lefèbvre, Phys. Rev. B **46**, 10 772 (1992).
[41] B. Vidal and P. Vincent, Appl. Opt. **23**, 1784 (1984).
[42] L. Sève, F. Bartolomé, J.M. Tonnerre, G. Patrat, D. Raoux, Y. Souche, V. Chakarian, and C. C. Kao (unpublished).
[43] C.T. Chen, Y.U. Idzerda, H.J. Lin, N.V. Smith, G. Meigs, and E. Chaban, Phys. Rev. Lett. **75**, 152 (1995).
[44] S. Andrieu, E. Foy, H. Fischer, M. Alnot, F. Chevrier, G. Krill, and M. Piecuch, Phys. Rev. B **58**, 8210 (1998).
[45] M.A. Tomaz, W.J. Antel, Jr., W.L. O'Brien, and G.R. Harp, Phys. Rev. B **55**, 3716 (1997).
[46] E.E. Fullerton, I.K. Schuller, H. Vanderstraeten, and Y. Bruynseraede, Phys. Rev. B **45**, 9292 (1992); E.E. Fullerton, J. Pearson, C.H. Sowers, S.D. Bader, X.Z. Wu, and S.K. Sinha, *ibid.* **48**, 17 432 (1993).
[47] H. Ardhuin, K. Suenaga, M.J. Casanove, E. Snoeck, C. Colliex, H. Fischer, S. Andrieu, and M. Piecuch, Phys. Rev. B **58**, 14 135 (1998).
[48] G.L. Krasko and G.B. Olson, J. Appl. Phys. **67**, 4570 (1990).
[49] C. Paduani and J.C. Krause, Phys. Rev. B **58**, 175 (1998).
[50] P. Radhakrisna and F. Livet, Solid State Commun. **25**, 597 (1978).
[51] H.R. Child and J.W. Cable, Phys. Rev. B **13**, 227 (1976).
[52] F. Kajzar and G. Parette, Phys. Rev. B **22**, 5471 (1980).
[53] M.F. Collins and G.G. Low, Proc. Phys. Soc. London **86**, 535 (1965).
[54] H. Akaï, M. Akaï, and J. Kanamori, J. Phys. Soc. Jpn. **54**, 4257 (1985).
[55] V.I. Anisimov, V.P. Antropov, A.I. Liechtenstein, V.A. Gubanov, and A.V. Postnikov, Phys. Rev. B **37**, 5598 (1988).
[56] B. Drittler, N. Stephanou, S. Blügel, R. Zeller, and P.H. Dederichs, Phys. Rev. B **40**, 8203 (1989).